Inorganic Chemistry

Article

pubs.acs.org/IC

On the Stereochemical Inertness of the Auride Lone Pair: Ab Initio Studies of AAu (A = K, Rb, Cs)

Maosheng Miao,[†,‡] Jakoah Brgoch,[†] Aditi Krishnapriyan,[§] Abby Goldman,[⊥] Joshua A. Kurzman,[∥] and Ram Seshadri*[,†,⊥,∥]

[†]Materials Research Laboratory, [§]Chemistry Program, College of Creative Studies, [⊥]Materials Department, [∥]Department of Chemistry and Biochemistry, University of California, Santa Barbara (UCSB), Santa Barbara, California 93106, United States

[‡]Beijing Computational Science Research Center, Beijing 10089, People's Republic of China

Supporting Information

ABSTRACT: The "lone" 6s electron pair often plays a key role in determining the structure and physical properties of compounds containing sixth-row elements in their lower oxidation states: Tl^{+}, Pb^{2+}, and Bi^{3+} with the $[Xe]4f^{14}5d^{10}6s^{2}$ electronic configuration. The lone pairs on these ions are associated with reduced structural symmetries, including ferroelectric instabilities and other important phenomena. Here we consider the isoelectronic auride Au^{-} ion with the $[Xe]4f^{14}5d^{10}6s^{2}$ electronic configuration. Ab initio density functional theory methods are employed to probe the effect of the 6s lone pair in alkali-metal aurides (KAu, RbAu, and CsAu) with the CsCl structure. The dielectric constants, Born effective charges, and structural instabilities suggest that the 6s lone pair on the Au^{-} anion is stereochemically inert to minor mechanical and electrical perturbation. Pressures greater than 14 GPa, however, lead to reorganization of the electronic structure of CsAu and activate lone-pair involvement and Au−Au interactions in bonding, resulting in a transformation from the cubic CsCl structure type to an orthorhombic *Cmcm* structure featuring zigzag Au−Au chains.

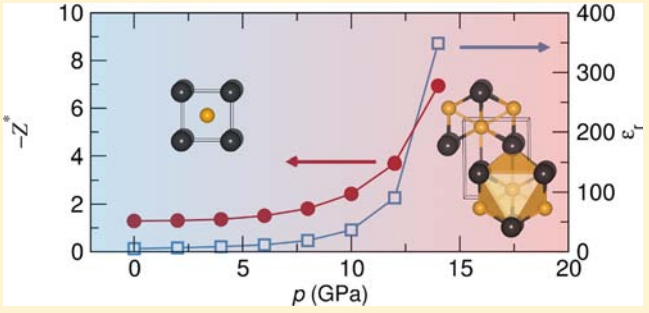

INTRODUCTION

Many aspects of the complex crystal chemistry and physical properties observed in compounds containing Au are often due to large relativistic effects.[1−4] Relativistic effects contract the 6s orbital of Au significantly, resulting in the unusually high (for a metal) electron affinity (EA) of 2.30 eV. For comparison, the EA of Ag is 1.30 eV and that of Cu 1.22 eV.[5] The high EA allows Au to become negatively charged (i.e., form Au^{-}) when surrounded by more electropositive elements. The simplest compounds containing the auride anion are AAu (A = K, Rb, Cs), which crystallize in the CsCl-type structure.[6−11] Other compounds containing anionic Au have also been reported, including A_3AuO (A = K, Rb, Cs)[12,13] and Ba_8As_5Au[14] as well as a number of other compounds.[15]

Besides the unusual charge state of Au, CsCl-type aurides and their alloys possess remarkable properties. For example, in the binary AAu (A = K, Rb, Cs), the properties change from metallic for KAu to semiconducting for RbAu and CsAu, with CsAu having a band gap of ≈2.6 eV.[7,8,16] This behavior of Au allows for a range of applications, from modification of the Schottky contact height at Au contacts with semiconductors[17] to the improvement of field-emission properties.[18] The presence of Au^{-} anions is also potentially important in catalytic processes considering that alkali metals such as Cs are used as promoters of Au catalysis,[19,20] although recent studies suggest that anionic Au species do not necessarily possess d states in the energy range appropriate for catalysis.[21]

In addition to being one of the few transition metals that can have a formal negative charge, the resulting Au^{-} also contains a 6s lone electron pair. Because lone pairs are easily polarized, compounds containing them have a strong propensity to respond to both mechanical and electric field perturbations.[22−26] Properties that originate from polarized lone pairs include (i) large static dielectric constants, (ii) large Born effective charges, (iii) large longitudinal- and transverse-optical (LO−TO) phonon splitting at the Γ point, (iv) ferroelectric and other polar instabilities, and (v) an inclination toward structural change under strain.

A notable example of a structure dictated by polarization of a lone pair is the deformation of litharge, α-PbO, away from the highly symmetric CsCl-type structure. This is due to polarization of the Pb^{2+} 6s lone pair caused by a hybridization between the Pb 6s lone pair and the O 2p orbitals.[27−30] In the case of TlX (X = Cl, Br, I), Tl^{+} contains a 6s lone pair similar to Pb^{2+} in α-PbO, yet it crystallizes in the CsCl-type structure even though recent work has shown the 6s lone pairs are still prone to polarization.[31] These thallium halides, in the absence of a structural distortion, still develop large static dielectric

Received: April 16, 2013
Published: July 3, 2013

   dx.doi.org/10.1021/ic400947p | Inorg. Chem. 2013, 52, 8183−8189

constants and Born effective charges close to 2+, which is twice the expected nominal charge (1+). It is also known that thallium halides have large LO−TO splitting and are close to ferroelectric instability. From the structures and properties of compounds that contain Tl^+ and Pb^{2+}, it is certain that understanding the polarizability of the 6s lone pair is essential to understanding the structures of their compounds and responses to external perturbations.

In this contribution, we apply ab initio density functional theory (DFT) methods on the binary system AAu (A = K, Rb, Cs) to understand the proclivity of the Au^- lone pair for polarization. This is investigated by calculating the dielectric constants, the Born effective charge, and the LO−TO phonon splitting. Additionally, the structural response to large perturbative stresses (either mechanical or electrical) is investigated. A transition under compressive pressure is identified in CsAu from the cubic phase to a new orthorhombic phase, which is due, in part, to greater 6s involvement in covalent bonding. The results suggest that the auride Au^- anion is largely stereochemically inert, at least at normal pressures, and is quite distinct from Tl^+, Pb^{2+}, and Bi^{3+}.

COMPUTATIONAL DETAILS

All calculations were performed in the framework of DFT using the Vienna ab Initio Simulation Package (VASP),[32,33] in which the wave functions are described by a plane-wave basis and the ionic potential is described by the projector augmented wave potentials.[34,35] This study considers three alkali-metal auride system, AAu (A = K, Rb, Cs), in the CsCl-type structure. Although KAu is believed to exist at high pressures, the structural optimization from the related structures provides accurate lattice parameters and properties for comparison here. The cubic lattice constants for all three systems, which are the only free structural parameters in a CsCl-type structure, were optimized using an 8 × 8 × 8 Monkhorst−Pack k mesh and a cutoff energy of 550 eV.[36,38−44] The effect of spin−orbit interaction (SOI) on determination of the structural stability was also examined. The total energies of the CsCl-type structure and the *Cmcm*-type structure were calculated using the complete SOI implementation in VASP. Because the calculations of forces and stresses are not implemented, the geometry obtained with PBE optimization in the absence of SOI was employed in these static calculations. In other words, SOI was not coupled in any way with structural relaxation.

Calculating the polarization-related properties, such as static dielectric constants and ferroelectric instability, strongly depends on the charge redistribution, which is well captured by the Perdew−Burke−Ernzerhof generalized gradient approximated (PBE-GGA) functional. Therefore, the PBE-GGA exchange-correlation functional and a cutoff energy and k mesh as described above are employed for these property calculations. The macroscopic dielectric properties and Born effective charges were calculated using the Berry phase formalism and the application of a small electric field, including the local field effect.[45,46] The Born effective charge tensor (Z^*) is the response of polarization due to a perturbation in the system. It is defined in eq 1

$$Z_{\alpha\beta}^{*} = \Omega \left.\frac{\partial P_\beta}{\partial u_\alpha}\right|_{\mathcal{E}=0} \quad (1)$$

where Ω is the primitive cell volume, P_β is the macroscopic polarization per unit cell, u is the displacement along the direction α, and $\mathcal{E}$ is the applied electric field.[47] The amplitude of Z^* governs the splitting between the longitudinal-optical (LO) and transverse-optical (TO) phonon modes. Phonon spectra, including the LO−TO splitting,[48] were calculated by density functional perturbation theory (DFPT)[49,50] with corrections to the LO−TO splitting.

To thoroughly examine the phase transitions of CsAu under compressive and tensile pressures, a structural search of the entire configuration space was conducted by a particle-swarm optimization (PSO) algorithm, as implemented in the *CALYPSO* code.[51] A system containing two Cs atoms and two Au atoms under ambient conditions and under compressive and tensile pressures was constructed. Here, 30 generations of structures were optimized, with each generation containing 50 structures. For a final comparison, structures were selected from both known binary compounds (AAu; A = K, Rb, Cs) and *CALYPSO* search results. Their enthalpies under external pressures ranging from −2 to +20 GPa were then calculated and compared against those of the ground-state structure of AAu (A = K, Rb, Cs) in the CsCl-type structure.

RESULTS AND DISCUSSION

Atomic and Electronic Structures. The optimized cubic lattice constants for the three alkali-metal aurides examined are given in Table 1 along with the experimentally determined values for RbAu and CsAu. The respective lattice constants are 2% and 3% larger than the reported experimental values for these two systems. The increase in lattice parameters when going down down the alkali metal column is expected based on the increasing ionic radii from K^+ (1.51 Å; eight-coordinated) to Rb^+ (1.61 Å; eight-coordinated) to Cs^+ (1.71 Å; eight-coordinated).[52]

Table 1. Lattice Constants of Optimized Structures of Alkali Metal, including KAu, RbAu, and CsAu in Comparison with Experimental Values

	PBE-GGA (Å)	experimental (Å)
KAu	4.043	
RbAu	4.222	4.107[9]
CsAu	4.376	4.262,[53] 4.241[53]

The electronic band structures for the optimized alkali-metal aurides indicate that KAu, RbAu, and CsAu are all semiconductors with indirect gaps between the R point at the valence band maximum and the X point at the conduction band minimum, which is in agreement with previously reported band-structure calculations.[41] KAu has the narrowest band gap of approximately 0.1 eV. Moving down the periodic table causes the (PBE) band gap to widen as the virtual Au 6p orbitals and alkaline-earth *ns* orbitals shift higher in energy. For instance, RbAu has a calculated band gap of ≈0.5 eV, whereas for CsAu, it is nearly 1 eV. Because a reduction of the band gap commonly occurs when using the PBE functional, the band gaps for these compounds are likely larger than those reported here.

Projecting the partial density of states (PDOS) into their component atomic orbitals, as shown in Figure 1, indicates that the Au 5d band is filled with a narrow dispersion in KAu between −3.5 and −2.25 eV. The d bands become even narrower upon going down the periodic table with bandwidths of ≈1 and 0.5 eV for RbAu and CsAu, respectively, because of the increasing Au−Au distances and limited orbital overlap. The alkaline-metal s and p orbitals are also in the conduction band and have a wide distribution across a 10 eV energy window. Above the Fermi level (E_F), the 6p orbitals of Au have a broad contribution above +1 eV and a band center approximately 5 eV higher in energy than the center of the Au 6s states, indicating minimal hybridization. Regardless, in RbAu and CsAu, it is clear from the electronic structure that the primary hybridization occurs between the Au^- 6s lone pair and the Au^- 5d states. Considering that orbital overlap between the cation and anion is limited in the aurides, the lone pair does not

dx.doi.org/10.1021/ic400947p | Inorg. Chem. 2013, 52, 8183−8189

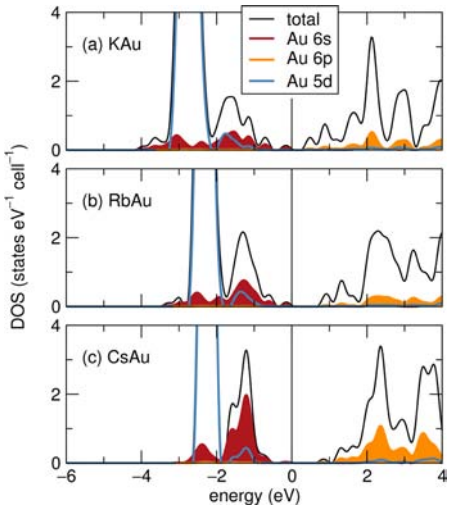

Figure 1. PDOS calculated for (a) KAu, (b) RbAu, and (c) CsAu with the CsCl-type structure. The Au 6s orbital densities of state are shown in red, the Au 6p in yellow, the Au 5d in blue, and the total DOS in black. E_F is set to 0 eV.

gain any directional character and thus is stereochemically inert, similar to a halide anion.

Calculated Dielectric Properties and Ferroelastic Instability. Even though the 6s lone pair of the auride anion is predicted to be stereochemically inactive based on the electronic structure, it is possible that there is still a strong dielectric response. To directly compare the dielectric properties of compounds with 6s lone pairs, the dielectric constants (ε_r) and Z^* are calculated. The resulting values for KAu, RbAu, and CsAu are presented in Table 2. Surprisingly, the calculated

Table 2. Polarization-Related Properties of Anionic Au$^-$ Compounds[a]

compound	ε_r	Z^* (Au)	ω_{TO} (cm^{-1})	ω_{LO} (cm^{-1})
KAu	6.18	−1.38	92.7	120
RbAu	5.32	−1.20	60.0	81.7
CsAu	4.93	−1.24	47.7	63.7

[a]The properties include the static dielectric constants (ε_r), the Born effective charges (Z^*), and the LO−TO phonon frequencies (ω_{LO} and ω_{TO}) at the Γ point.

dielectric constants for the aurides are all close to the modest values of alkali halides. For example, the ε_r values of KAu, RbAu, and CsAu are 6.18, 5.32, and 4.93, respectively, which are similar to the ε_r values in NaCl (5.72), NaBr (6.44), CsBr (6.38), and CsI (6.31).[54] Because alkali halides are prototypical ionic compounds, a nearly complete electron transfer between the cation and anion leads to filled valence electron shells. With fully occupied orbitals, the halides are resistant to polarization, leading to their small dielectric constants. Referring to the electronic structure presented in Figure 1, this is also the case for the auride compounds. The 6s and 5d orbitals of all three compounds are nearly filled owing to the relatively high electronegativity of Au limiting the dielectric response. In a system that is known to have active lone pairs, such as TlCl and TlBr, the dielectric constants are nearly 10-fold larger, with respective ε_r values of 32 and 30 at room temperature.

The Born effective charge is also an indicator of the dielectric properties because it arises from a response to a change in the external field. In the halides, Z^* is usually close to its nominal charge state of 1−. For example, the Z^* value of Cl^- in NaCl is −1.10, as measured experimentally,[55] and −1.15, as calculated by the Berry phase method.[56] The agreement between the Born effective charge and the valence state of the anion is consistent with the fact that halogen anions are not polarizable. As shown in Table 2, the calculated Born effective charges for the auride compounds KAu, RbAu, and CsAu are −1.38, −1.20 and −1.24, a result that supports a weak tendency for polarization of the Au^- 6s lone pair. For comparison, the Z^* values for TlX (X = Cl, Br, I) are all approximately ±2, double the expected value for Tl^+X^-.[31] Again, the large Z^* values in the TlX compounds are theorized to stem from cross-gap hybridization between the halide *n*p orbitals and the Tl 6p orbitals, which is not present in the AAu (A = K, Rb, Cs) system (Figure 1). Nevertheless, the Z* values presented in Table 2 are still larger than those of the halides, meaning that these compounds could be on the verge of instability under moderate perturbation.

Another method for analyzing the activity of the lone pair is through the splitting of the LO−TO phonon frequencies. The resulting phonon band structure for CsAu is shown in Figure 2.

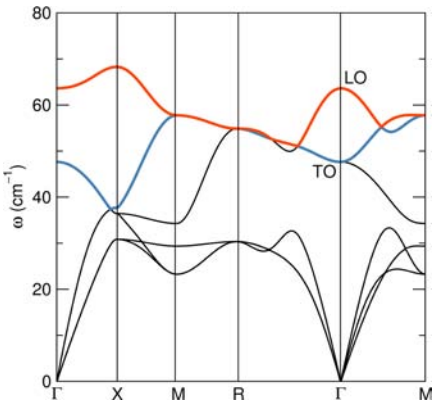

Figure 2. Phonon spectra of CsAu calculated by DFPT showing the LO (orange) and TO (blue) phonon branches, with the remaining branches (one optical and three acoustic) in black. This is in agreement with the previous reported phonon spectra.[39].

RbAu and KAu are qualitatively the same. There are six branches of phonon modes, including three acoustic phonons and three optical phonons. All three acoustic phonons are degenerate and have 0 frequency at the Γ point. The degeneracy of the optical phonons is broken between the R and Γ points, with the LO phonon frequency becoming higher in frequency than the TO phonon at the Γ point. This is a unique feature of ionic crystals and is caused by the emergence of a macroscopic electric field in the LO phonon in a long-wavelength limit. In ionic compounds containing stereochemically active lone pairs, the atomic displacement associated with the long-wavelength LO phonon modes may induce very strong polarization fields and therefore the LO−TO phonon splittings are usually exceedingly large in these systems. The LO−TO splitting of the alkali-metal aurides, as shown in Table 2, are similar to those encountered in alkali-metal halides.[57] These are much smaller than the TlX (X = Cl, Br, I) compounds, which have a $\omega_{LO}-\omega_{TO}$ splitting between ≈50 and 100 cm^{-1}. These are approximately 3−5 times larger than the calculated splitting for the aurides.[31]

Because these auride compounds have small Born effective charges, low dielectric constants, and a small LO−TO splitting,

dx.doi.org/10.1021/ic400947p | Inorg. Chem. 2013, 52, 8183−8189

a ferroelectric instability would not be predicted like with the thallium halide compounds.[31] To confirm if these indicators are correct, the ferroelectric instability is calculated. The total energy of CsAu is calculated with a displacement of Au^- anions along the [100], [110], and [111] directions, while the crystal lattice is under homogeneous strain ranging from −3% (compressive) to +3% (tensile). As shown in Figure 3, the

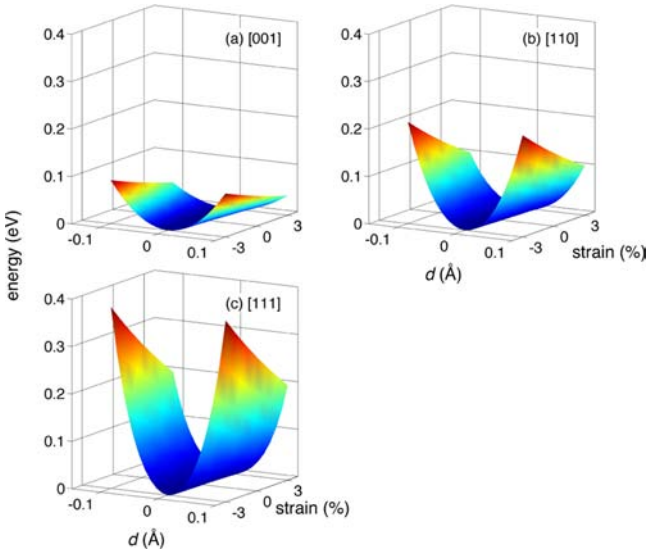

Figure 3. Contour plots of the total energies of CsAu as a function of the displacements of Au atoms along [100], [110], and [111] orientations. Calculations are performed for the PBE-optimized lattice as well as lattices under both compressive (negative) and tensile (positive) strains up to 3%.

total energy increases monotonically with an increase of the displacement of the Au^- anion in all three directions throughout the whole strain range studied. The changes in energy for these three directions are predominantly due to the Coulombic and repulsive interactions between the Au anions and Cs cations, with the least densely packed plane, (001), having the smallest energy change and the most densely packed plane, (111), having the largest energy change. If a ferroelectric instability were present in the structure, when atoms shift from the center, a decrease in energy would be expected under strain, making it more energetically favorable compared to the zero-strain structure. However, from these results, it is clear that the values are always positive, further confirming that Au^- anions behave strikingly like charged hard spheres even under perturbation.

Predicting a High-Pressure Phase for CsAu. The 6s lone pair of the auride anion (in the CsCl-type structure) is stereochemically inert to minor external mechanical and electrical perturbations, as is evident based on the small Z^*, ε_r, and LO−TO splittings. However, when exposed to larger stresses, such as high pressure, it is possible that the lone pair will become active, leading to structural distortion. To determine if a different structure is more favorable under high pressure, candidate structures, illustrated in Figure 4, were selected from the Inorganic Crystal Structure Database and an automatic search of the structural configuration space using a PSO algorithm.

The total energies of these structures were calculated as a function of the external pressure and plotted relative to the total energy of CsAu in the CsCl-type structure (Figure 5a).

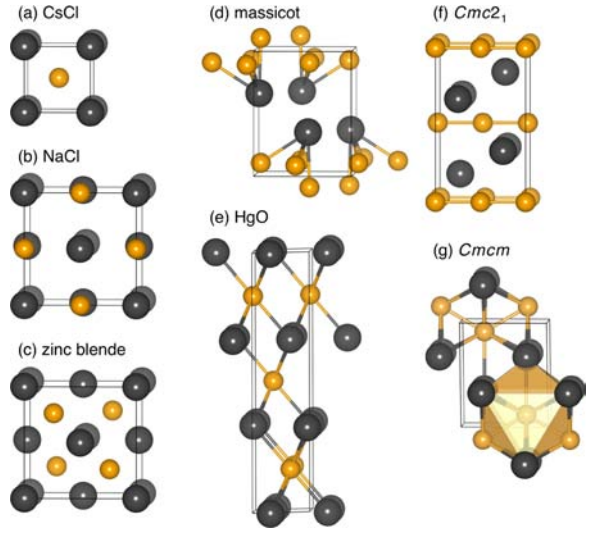

Figure 4. Structures of Au anion compounds including (a) CsCl-type structure, (b) NaCl-type structure, (c) zinc blende, (d) massicot, β-PbO -type, (e) $P3_121$ structure, HgO-type, (f) $Cmc2_1$ (PSO search), and (g) *Cmcm*, CrB-type (PSO search).

Under small tensile pressure, the structures with lower coordination numbers, such as rock salt NaCl (Figure 4b) and zinc blende (Figure 4c), become lower in energy than the CsCl-type structure. Stabilization of these structures is likely due to optimization of bonding interactions by a slight expansion of the unit cell. In these structures, there is no sign of polarization of the Au^- 6s electrons. The dielectric constants and Born effective charges are similar to those of the CsCl structure.

Under compressive pressure from 0 to 14 GPa, CsAu in the CsCl-type structure is the lowest-energy structure. Each additional structure type modeled has a higher relative total energy (favors the CsCl-type structure) at increased pressures. The energy of the low-coordination structures, NaCl-type and zinc blende-type structures, increase dramatically with pressure, having relative total energies of 1 and 2.25 eV higher than that of the CsCl-type structure at 10 GPa. The relative total energies of the other structures, including CsAu in the PbO-type massicot (*Pbcm*) structure (Figure 4d), CsAu in the HgO-type ($P3_121$) structure (Figure 4e), and a structure determined using PSO that forms a $Cmc2_1$ structure (Figure 4f), all have a smaller difference in the relative total energy at higher pressure but are never favored. The relative total energy of the *Cmcm*-type structure (Figure 4g), found by a PSO search, increases with pressure initially and then decreases, causing the *Cmcm* structure to become more energetically favorable than the CsCl-type CsAu. Across the entire pressure range, the energy difference between this structure and the CsCl-type structure is very small. In fact, at 2 GPa, the energy of the *Cmcm* structure is only 1 meV larger than that of the CsCl-type structure. Such a small difference in the total energy means that at only slightly elevated pressures and moderate temperatures a structural distortion might be observed experimentally.

With such a small total energy difference between the structure types, it is possible that SOI could play a role in determining the preferred structure.[37] The geometry optimization/structure relation is not implemented in the full SOI calculation, and thus we employ the non-SOI PBE-optimized geometry for static total energy calculations with SOI. As

dx.doi.org/10.1021/ic400947p | Inorg. Chem. 2013, 52, 8183−8189

shown in Figure 6, the inclusion of SOI decreases ΔE by ≈25 meV across the entire pressure range. Because of SOI, the

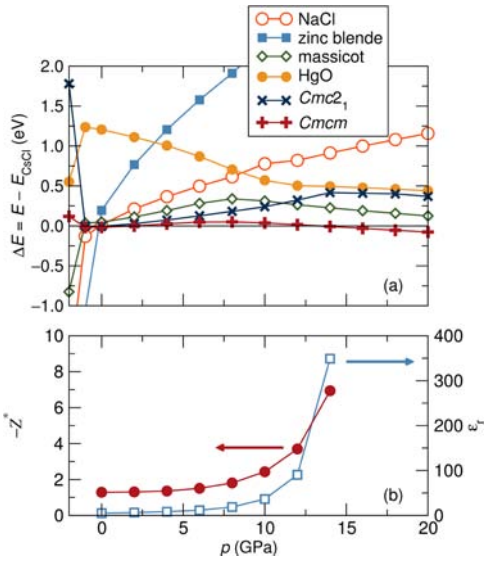

Figure 5. (a) Total energy as a function of external pressure for selected structures of CsAu in the structure types NaCl (circles), zinc blende (squares), massicot PbO (diamonds), HgO (filled circles), PSO-search $Cmc2_1$ (×), and PSO-search *Cmcm* (+) relative to the total energy of the CsCl-type structure (solid black line; $\Delta E = E_{model} - E_{CsCl\text{-}type}$). (b) (Negative) Born effective charge ($-Z^*$) for Au^- (red circles) and the dielectric constant (ε_r; blue squares) calculated for CsAu in the CsCl-type structure as a function of the pressure.

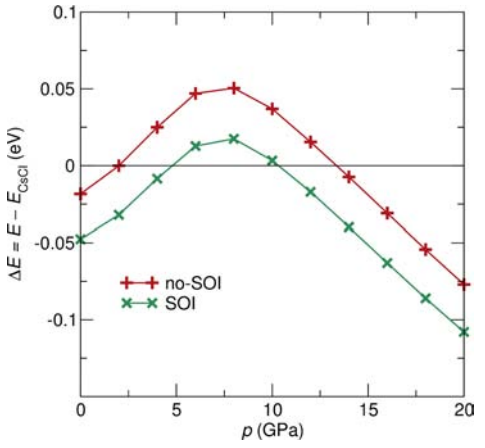

Figure 6. Energetic stabilization of the *Cmcm*-type structure calculated as a function of the external pressure without SOI (red, +) and with SOI (green, ×) relative to the total energy of CsCl-type (solid black line) with and without SOI ($\Delta E = E_{model} - E_{CsCl\text{-}type}$).

transition pressure from the CsCl-type structure to the *Cmcm* structure occurs around 10 GPa. At pressures below 5 GPa, it appears that the *Cmcm*-type structure is also preferred over the CsCl-type structure; however, when all of the structures are considered (Figure 5), *Cmcm* is not the lowest-energy structure at ambient pressures. The results including SOI must be interpreted with reservation because they were determined using the structural parameters obtained using the PBE functional without SOI. Although the limited free structural parameters in the CsCl-type structure would allow for optimization with SOI, this is not the case for the orthorhombic *Cmcm*-type structure. Nevertheless, a structural transition between these two structure types is predicted to occur between 10 and 14 GPa. The identification of a pressure-induced phase transformation is in agreement with previous experimental observations. Using Mössbauer spectroscopy on ^{197}Au, a phase change in **CsAu** was identified at 4.2 K and approximately 3 GPa to a lower-symmetry structure, although the exact structure was not identified.[58] Additionally, total energy calculations indicate a pressure-induced phase transition at ≈4.5 GPa from the CsCl-type structure to the lower-symmetry NaTl-type structure.[59] CsAu in the NaTl-type structure was also modeled here; however, the total energy difference greatly favored (by at least +1 eV) the CsCl-type structure across the pressure range probed.

If the predicted distortion is driven by activation of the Au^- 6s lone pair under a large perturbation, the polarization properties will be a strong indicator. Upon calculation of Z^* and ε_r for CsAu in the CsCl-type structure as a function of the pressure, it is clear that changes in the lone pair occur as a function of the pressure. For example, at low pressure, <8 GPa, Z^* and ε_r maintain values similar to those determined in the ground-state structure. Increasing the pressure beyond 8 GPa leads to an abrupt increase in the polarization properties. The result is a $-Z^*$ value of ≈7 and an ε_r value of nearly 380 at 14 GPa. These values are much higher than the values reported for the thallium halide compounds. Accordingly, the predicted pressure-induced phase transformation from the high-symmetry CsCl-type structure to a *Cmcm*-type structure is concomitant with activation of the 6s lone pair.

The *Cmcm* structure is isostructural with the CrB-type structure,[60] with Cs on the Cr site and Au on the boron site. There are only minor structural differences between this new structure and the CsCl-type structure. In the *Cmcm* structure, Au^- has seven neighboring Cs atoms compared to the eight nearest-neighboring Cs atoms in the CsCl-type structure. At 0 GPa, the Cs−Au bond distances in the *Cmcm* structure are 3.654 Å, 3.753 Å, and 3.849 Å. The next-nearest-neighboring Cs^+ ions are more than 6 Å from the Au^- ions. These Cs−Au bond distances are similar to those in the CsCl-type structure, which are 3.794 Å, as optimized using the PBE functional. The nearest-neighboring Cs−Cs distance in the *Cmcm* structure is 4.381 Å, nearly identical with that of the CsCl-type structure. The major difference between the two structures is the Au−Au bond distance. In the *Cmcm* structure, the Au−Au interaction is 3.034 Å, significantly smaller than that in the CsCl-type structure (4.381 Å). In fact, this distance is only slightly larger than the Au−Au bond in *fcc*-Au at ambient pressure. The short Au−Au bonds in the *Cmcm* structure lead to the formation of Au−Au zigzag chains along the *c* direction (Figure 4g). This structural motif is similar to the ternary system A_2AuN (A = Ca, Sr), which also contains Au−Au zigzag chains with similar bond distances (2.86 and 3.05 Å).[61,62] Therefore, this structure preference appears to be driven not only by the activity of the lone pair but also by the intrinsic aurophilicity.[63]

Analysis of the electronic structure in the *Cmcm*-type CsAu indicates rather large changes compared to the CsCl-type structure. Most notably, the high-pressure phase is predicted to be a (poor) metal rather than a semiconductor. The atomic rearrangements, leading to the short Au−Au distance, cause a larger dispersion of the Au 5d bands between −5.5 and ≈−0.5 eV. There is also significant hybridization of 6s and 5d orbitals due to the neighboring Au anions. The *Cmcm* structure also has 5d states above E_F overlapping with the Au 6p states,

dx.doi.org/10.1021/ic400947p | Inorg. Chem. 2013, 52, 8183−8189

something not observed in the CsCl-type structure. The Au 6p bands in the *Cmcm* structure are also delocalized across the entire energy window plotted in Figure 7. The result is the loss of a band gap and formation of a broad pseudogap ranging between −1 and 1 eV.

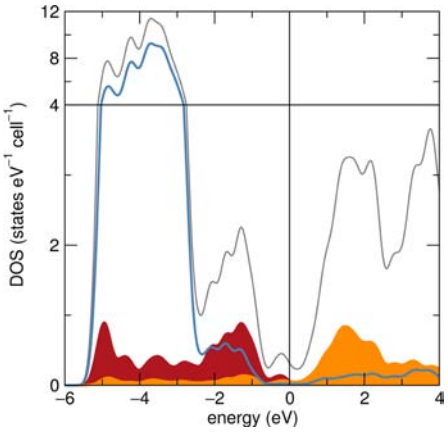

Figure 7. DOS of CsAu in the *Cmcm* structure found using the PSO method at 14 GPa. The geometry and electronic structure are calculated by the PBE functional. The total DOS is gray, Au 5d orbitals are blue, Au 6s orbitals are red, and Au 6p orbitals are yellow. E_F is set to 0 eV.

CONCLUSIONS

Ab initio calculations are employed to determine the properties of the alkali-metal aurides including KAu, RbAu, and CsAu in the CsCl-type structure. From the static dielectric constants, the Born effective charges, and the LO−TO splitting, it is possible to show that the 6s lone pair in Au^- is stereochemically inert and does not dictate the structural chemistry of these simple binary compounds. In fact, ε_r, Z^*, and the LO−TO splitting all have values that are closer to alkali-metal halides rather than thallium halides. The lack of stereochemical activity on these compounds can be explained by the absence of orbital mixing between A^+ and Au^-. Although hybridization between the s and d orbitals occurs for Au^-, it does not yield the same lone-pair activity as cation−anion orbital mixing, which is in contrast to previous theories.[64] Finally, increasing the strain on the CsAu system is associated with a large increase in Z^* and ε_r. The result is a pressure-induced phase transformation at 14 GPa. This new high-pressure phase crystallizes as an orthorhombic structure (*Cmcm*) and contains infinite Au−Au zigzag chains.

ASSOCIATED CONTENT

Supporting Information

Crystallographic data for the seven binary Cs−Au structure types explored in this study. This material is available free of charge via the Internet at http://pubs.acs.org.

AUTHOR INFORMATION

Corresponding Author

*E-mail: seshadri@mrl.ucsb.edu.

Notes

The authors declare no competing financial interest.

ACKNOWLEDGMENTS

This work was supported by the National Science Foundation (NSF; Grant DMR-110530). The work made use of the computing facilities of the Center for Scientific Computing supported by the California Nanosystems Institute (Grant CNS-0960316), Hewlett-Packard, and by the Materials Research Laboratory at UCSB: an NSF MRSEC (Grant DMR-1121053). Part of the calculations also made use of computing facilities supported by the NSF-funded XSEDE under Grant TG-DMR130005. A.K. has been supported by the RISE Program (Grant DMR-1121053).

REFERENCES

(1) Pitzer, K. S. *Acc. Chem. Res.* **1979**, *12*, 271−276.
(2) Pyykkö, P. *Angew. Chem., Int. Ed.* **2002**, *41*, 3573−3578.
(3) Jansen, M. *Chem. Soc. Rev.* **2008**, *37*, 1824−1835.
(4) Pyykkö, P. *Annu. Rev. Phys. Chem.* **2012**, *63*, 45−64.
(5) Hotop, H.; Lineberger, W. C. *J. Phys. Chem. Ref. Data* **1985**, *14*, 731−750.
(6) Sommer, A. *Nature* **1943**, *152*, 215−215.
(7) Spicer, W.; Sommer, A.; White, J. *Phys. Rev.* **1959**, *115*, 57−62.
(8) Liu, T. *Phys. Rev. B* **1975**, *12*, 3008−3012.
(9) Tinelli, G.; Holcomb, D. *J. Solid State Chem.* **1978**, *25*, 157−168.
(10) Busse, B.; Weil, K. *Phys. Chem. Chem. Phys.* **1981**, *85*, 309−313.
(11) Zachwieja, U. *Z. Anorg. Allg. Chem.* **1993**, *619*, 1095−1097.
(12) Feldmann, C.; Jansen, M. *Angew. Chem., Int. Ed. Engl.* **1993**, *32*, 1049−1050.
(13) Feldmann, C.; Jansen, M. *Z. Anorg. Allg. Chem.* **1995**, *621*, 201−206.
(14) Nuss, J.; Jansen, M. *Z. Kristallogr. NCS* **2002**, *217*, 313−314.
(15) Hensel, F. *Z. Phys. Chem. N. F.* **1987**, *154*, 201−219.
(16) Wooten, F.; Condas, G. *Phys. Rev.* **1963**, *131*, 657−659.
(17) Wertheim, G.; Rowe, J.; Chiang, C.; Malic, R.; Buchanan, D. *Surf. Sci.* **1995**, *330*, 27−33.
(18) Bernatskii, D. P.; Pavlov, V. G. *Tech. Phys. Lett.* **2006**, *32*, 579−581.
(19) Vansanten, R.; Kuipers, H. *Adv. Catal.* **1987**, *35*, 265−321.
(20) Zomerdijk, J.; Hall, M. *Cat. Rev., Sci. Eng.* **1981**, *23*, 163−185.
(21) Miao, M.-S.; Kurzman, J. A.; Mammen, N.; Narasimhan, S.; Seshadri, R. *Inorg. Chem.* **2012**, *51*, 7569−7578.
(22) Cohen, R. *Nature* **1992**, *358*, 136−138.
(23) Seshadri, R. *Proc. Indian Acad. Sci. Chem. Sci.* **2001**, *113*, 487−496.
(24) Seshadri, R.; Hill, N. *Chem. Mater.* **2001**, *13*, 2892−2899.
(25) Waghmare, U. V.; Spaldin, N. A.; Kandpal, H. C.; Seshadri, R. *Phys. Rev. B* **2003**, *67*, 125111.
(26) Stoltzfus, M. W.; Woodward, P. M.; Seshadri, R.; Klepsis, J.-H.; Bursten, B. *Inorg. Chem.* **2007**, *46*, 3839−3850.
(27) Walsh, A.; Payne, D. J.; Egdell, R.; Watson, G. W. *Chem. Soc. Rev.* **2011**, *40*, 4455−4463.
(28) Watson, G. W.; Parker, S. C.; Kresse, G. *Phys. Rev. B* **1999**, *59*, 8481−8486.
(29) Watson, G. W.; Parker, S. C. *J. Phys. Chem. B* **1999**, *103*, 1258−1262.
(30) Raulot, J.-M.; Baldinozzi, G.; Seshadri, R.; Cortona, P. *Solid State Sci.* **2002**, *4*, 467−474.
(31) Du, M.-H.; Singh, D. J. *Phys. Rev. B* **2010**, 81.
(32) Kresse, G.; Hafner, J. *Phys. Rev. B* **1993**, *47*, 558−561.
(33) Kresse, G.; Furthmuller, J. *Phys. Rev. B* **1996**, *54*, 11169−11186.
(34) Blöchl, P. *Phys. Rev. B* **1994**, *50*, 17953−17979.
(35) Kresse, G.; Joubert, D. *Phys. Rev. B* **1999**, *59*, 1758−1775.
(36) Baldereschi, A.; Meloni, F. *Helv. Phys. Acta* **1976**, *49*, 160.
(37) Miao, M.-S.; Seshadri, R. *J. Phys.: Condens. Matter* **2012**, *24*, 215503.
(38) Christensen, N.; Kollar, J. *Solid State Commun.* **1983**, *46*, 727−730.

(39) Erdinc, B.; Soyalp, F.; Akkus, H. *Cent. Eur. J. Phys.* **2011**, *9*, 1315−1320.
(40) Hasegawa, A.; Watabe, M. *J. Phys. F: Met. Phys.* **1977**, *7*, 75−86.
(41) Koenig, C.; Christensen, N.; Kollar, J. *Phys. Rev. B* **1984**, *29*, 6481−6488.
(42) Norris, C.; Wallden, L. *Phys. Lett. A* **1969**, *A 30*, 247−&.
(43) Spicer, W. *Phys. Rev.* **1962**, *125*, 1297.
(44) Werthein, G.; Bates, C.; Buchanan, D. *Solid State Commun.* **1979**, *30*, 473−475.
(45) King-Smith, R. D.; Vanderbilt, D. *Phys. Rev. B* **1993**, *47*, 1651−1654.
(46) Vanderbilt, D.; King-Smith, R. D. *Phys. Rev. B* **1993**, *48*, 4442−4455.
(47) Ravindran, P.; Vidya, R.; Kjekshus, A.; Fjellvåg, H.; Eriksson, O. *Phys. Rev. B* **2006**, *74*, 224412.
(48) Togo, A.; Oba, F.; Tanaka, I. *Phys. Rev. B* **2008**, *78*, 134106.
(49) Baroni, S.; Resta, R. *Phys. Rev. B* **1986**, *33*, 7017−7021.
(50) Gajdos, M.; Hummer, K.; Kresse, G.; Furthmuller, J.; Bechstedt, F. *Phys. Rev. B* **2006**, *73*, 045112.
(51) Wang, Y.; Lv, J.; Zhu, L.; Ma, Y. *Phys. Rev. B* **2010**, 82.
(52) Shannon, R. *Acta Crystallogr., Sect. A* **1976**, *32*, 751−767.
(53) Kienast, G.; Verma, J.; Klemm, W. *Z. Anorg. Allg. Chem.* **1961**, *310*, 143−169.
(54) Sirdeshmukh, D. B.; Sirdeshmukh, L.; Subhadra, K. G. *Alkali halides: a handbook of physical properties*; Springer: Berlin, 2001; Vol. *49*.
(55) Sandgster, M.; Schoder, U.; Atwood, R. *J. Phys. C: Solid State* **1978**, *11*, 1523−1540.
(56) Mei, W.; Boyer, L.; Mehl, M.; Ossowski, M.; Stokes, H. *Phys. Rev. B* **2000**, *61*, 11425−11431.
(57) Falter, C.; Klenner, M.; Hoffmann, G. A.; Schnetgöke, F. *Phys. Rev. B* **1999**, *60*, 12051−12060.
(58) Stanek, J.; Hafner, S. S.; Hensel, F. *Phys. Rev. B* **1985**, *32*, 3129−3133.
(59) Christensen, N. E. *Phys. Rev. B* **1985**, *32*, 207−228.
(60) Kiessling, R. *Acta Chem. Scand.* **1949**, *3*, 595−602.
(61) Henry, P. F.; Weller, M. T. *Angew. Chem., Int. Ed.* **1998**, *37*, 2855−2857.
(62) Prots, Y.; Auffermann, G.; Kniep, R. *Z. Anorg. Allg. Chem.* **2002**, *628*, 2205.
(63) Schmidbaur, H. *Gold Bull.* **2000**, *33*, 3−10.
(64) Orgel, L. E. *J. Chem. Soc.* **1959**, *0*, 3815−3819.